

Magnetic fields in planetary nebulae and post-AGB nebulae

L. Sabin^{1,2}, Albert A. Zijlstra¹ and J. S. Greaves³

¹*Jodrell Bank Centre for Astrophysics, University of Manchester, P.O. Box 88, Manchester M60 1QD, UK*

²*Instituto de Astrofísica de Canarias, C/ Vía Láctea, 38205 Laguna, Tenerife, Canary Islands, Spain*

³*School of Physics & Astronomy, University of St. Andrews, North Haugh, St Andrews KY16 9SS, Scotland, UK*

17 September 2018

ABSTRACT

Magnetic fields are an important but largely unknown ingredient of planetary nebulae. They have been detected in oxygen-rich AGB and post-AGB stars, and may play a role in the shaping of their nebulae. Here we present SCUBA sub-millimeter polarimetric observations of four bipolar planetary nebulae and post-AGB stars, including two oxygen-rich and two carbon-rich nebulae, to determine the geometry of the magnetic field by dust alignment. Three of the four sources (NGC 7027, NGC 6537 and NGC 6302) present a well-defined toroidal magnetic field oriented along their equatorial torus or disk. NGC 6302 may also show field lines along the bipolar outflow. CRL 2688 shows a complex field structure, where part of the field aligns with the torus, whilst an other part approximately aligns with the polar outflow. It also presents marked asymmetries in its magnetic structure. NGC 7027 shows evidence for a disorganized field in the south-west corner, where the SCUBA shows an indication for an outflow. The findings show a clear correlation between field orientation and nebular structure.

Key words: stars: AGB and post-AGB – stars: mass-loss –method: polarimetry

1 INTRODUCTION

Whether magnetic fields play a role in the shaping of planetary nebulae (PNe) is an open question. Most of the post-AGB nebulae appear elliptical, bipolar or even multi-polar (Balick & Frank 2002). These morphologies are amplified by the interaction between a slow AGB wind with a faster post-AGB wind. However, this amplification still requires an initial asymmetry in the slow wind. This initial shaping has been mainly attributed to two possible phenomena: binarity and magnetic fields.

In the binary model, a close companion affects the mass-losing AGB star via common envelope evolution (De Marco & Moe 2006), mass transfer and/or tidal forces, and may lead to the formation of an accretion disk around the companion star. The binary orbit provides a source of angular momentum which get carried by the wind, and leads to an equatorial disk. The angular momentum loss by the stars may lead to a merger. The model of shaping due to this binary interaction is quite popular (Bond & Murdin 2000), (Ciardullo et al. 2005), partly because of the presumed impossibility for a single star to supply the energy necessary to create a magnetic field strong enough for its shaping (Soker 2005). Nevertheless, there is still a lack of observational evidence for the occurrence of close binary systems during the AGB phase. Neither companions (Riera et al. 2003) nor high orbital velocities of the AGB stars (Barnbaum et al. 1995) are detected in a sufficient amount to establish the role of the binarity as predominant (Matt et al. 2000). Evidence for binary

interactions may be found in 25–50 per cent of planetary nebulae (Zijlstra 2006), although values of 50–100 per cent have also been suggested (De Marco et al. 2004; De Marco & Moe 2006).

On the other hand, the magnetic field may act as a “squeezer” around the central star of the PN and thereby give the dust its direction (in the sense of the outflow). Magnetic fields have been detected around AGB stars (Vlemmings et al. 2006) and a few post-AGB stars (Bains et al. 2004) using radio observations of masers (H₂O, SiO, OH). Such observations measure a local value of the strength of field, within masing high-density clumps, which may differ from the global field. The origin of the magnetic field is unknown: a dynamo effect resulting from an interaction between a slow rotating envelope and a fast rotating core has been proposed (Blackman et al. 2001). As magnetic fields are now known to be present in the AGB and the post-AGB phase, their importance should not be ruled out prematurely.

Greaves (2002) found evidence for dust alignment in two carbon-rich objects, NGC 7027 and CRL2688 which are respectively a young and compact bipolar PN and a strongly bipolar proto-planetary nebula (PPN). This was based on polarimetric Scuba 850-micron observations. The data suggests the presence of toroidal collimated magnetic fields, as would be required for the shaping. But the presence of such a field was not conclusively proved, because of the very few detected vectors and limited spatial resolution. We present here new 850-microns and the first 450-microns polarimetry of post-AGB stars, which allows for better resolution and reduces angular smearing. In addition to the objects observed

by Greaves (2002), we also observed NGC 6537 and NGC 6302. The sample contains two carbon-rich and two oxygen-rich nebulae. We show the presence of well-aligned toroidal fields in three of the nebulae. The fourth object shows indications for both a toroidal field and one aligned with the polar outflow. We conclude that toroidal fields may be common in bipolar PNe, and could play a role in the shaping of the nebulae.

2 OBSERVATIONS

The polarimetric data have been obtained May 10th 2005, with the polarimeter on the Sub-millimeter Common-User Bolometer Array (SCUBA), at the JCMT. The instrument (now decommissioned) is described in Holland et al. (1999). The JCMT beam size is 15 arcsec at 850 μ m and 8 arcsec at 450 μ m.

SCUBA contains two arrays of bolometric detectors, covering a field of view of 2.3' in diameter. The 850- μ m array has 37 individual detectors, and the 450- μ m array has 91 detectors. The two arrays are used simultaneously. The spatial resolution of the detector is 7.5" at 450 μ m, and 14" at 850 μ m. The gaps between the detectors are covered by moving the telescope in sub-pixel steps, in the so-called jiggle-map mode. The step size needs to be optimized for the wavelength used. The polarimeter (Greaves et al. 2003) measures the linear polarization by rotating the half-waveplate in 16 steps. We used this in combination with jiggle map mode. A chopthrow of 45 arcsec was used.

Good photometric images cannot be obtained at both wavelengths simultaneously. When the jiggle pattern is optimized one wave-band, the simultaneous image obtained in the other band is under-sampled. The size of the pixels in the final image is set during the data reduction with the polarimetric package of Starlink. For a jiggle pattern corresponding to a 450 μ m measurement, the pixel spacing becomes 3 arcsec and for 850 μ m it is 6 arcsec. The reduction of infrared polarimetry is discussed in detail by Hildebrand et al. (2000).

The instrumental polarization (IP) of each detector has to be removed in order to have a correct polarization calibration. A new IP calibration, provided on site, was used: this contains a re-measurement of the central detector. For the other detectors, an older IP calibration was used. The IP should not vary too much for detectors close to the center of the array. Some tests done to see the importance of the instrumental polarization (by changing its value by the size of the error for example) and if it could affect the polarization vectors length, showed that in our case, the IP was small (at 850 μ m: $\sim 1.20\% \pm 0.25\%$ and at 450 μ m: $\sim 3.25\% \pm 0.25\%$) and didn't play any role in modifying the vectors. The resulting polarimetric images were checked for different pixel binning, from 1×1 to 10×10 , and we didn't find any significant changes.

The linear polarization is measured as a percentage polarization, and a direction. The polarization is typically caused by the alignment of spinning dust grains, with their long axis perpendicular to the local magnetic field (Greaves et al. 1999). Thus, the measured angle of polarization is 90 degrees rotated with respect to the magnetic field. The degree of polarization does not give direct information on the strength of the magnetic field.

We observed four targets: NGC 6537, CRL 2688, NGC 6302 and NGC 7027. They were observed in jiggle map observing mode at both wave-bands, 450 μ m and 850 μ m. For each object, the mean direction and angle of polarization are listed in Table 1.

The figures below show the direction of the magnetic field, i.e. the vectors are perpendicular to the direction of the grain alignment.

3 THE RESULTS

3.1 NGC 6537

NGC 6537 is also known as the Red Spider nebula. It is a bipolar planetary nebula with a very hot central star ($1.5\text{--}2.5 \times 10^5$ K). The nebula suffers extinction by circumstellar dust. This extinction is localized mainly in a compact circumstellar shell. An extinction map (Matsuura et al. 2005) reveals a compact dust shell with a roughly spherical inner radius of about 3 arcsec, with a minimum towards the central star (Matsuura et al. 2005; Cuesta et al. 1995). The polar outflows (traced by high velocity winds of about 300 km/s: Corradi & Schwarz 1993) extend 2 arcminutes along the NE-SW direction. The Scuba 850- μ m continuum map (Fig. 1) shows elongation perpendicular to the outflow direction, with a major-axis diameter of approximately 20 arcsec. The extinction map is now seen to represent the inner edge of a more extended, and possibly toroidal, structure. The equatorial plane may be oriented a little closer to the EW direction, based on the Scuba map.

The best polarimetric results obtained with SCUBA are obtained at 850 μ m. The consistent orientation of the polarization vectors shows that the magnetic field (hereafter \vec{B}) has a dominant direction along the equatorial plane, approximately perpendicular to the outflow direction. The dust alignment is therefore directed in the same sense as the outflow. The length of the 18 different vectors does not show large variations, with a degree of polarization varying from 8 to 14%, suggesting a consistent magnetic field. Moreover the absence of smaller polarization vectors toward the center of the nebula indicates that there is no change in geometry of \vec{B} towards the core (Greaves 2002). This supports a location some distance from the star (i.e. in a detached shell), since otherwise averaging of vectors in different directions within the JCMT beam would reduce the detected net polarization at the central position (beam depolarization).

These observations indicate the presence of a consistent toroidal magnetic field, located along the equatorial plane of NGC 6537, in a circumstellar torus. Compared to the size of the outflow lobes, the field is located relatively close to the star. The presence of a \vec{B} -field had already been suspected, based on the occurrence of filaments near the central star (Huggins & Manley 2005).

The extinction map obtained by Matsuura et al. (2005) (Fig. 1- Bottom panel) shows an asymmetry, in that the extinction is higher on the western side (≈ 2 mag versus ≈ 1.6 mag towards the east). This asymmetry is also seen in the Scuba data, with a larger extension and more polarization vectors on this side. This is a further indication that the magnetic field is located within the detached dust shell.

There is no strong indication for magnetic fields along the spider lobes. There is a slight trend for the vectors to curve, but this is caused by only a few of the vectors and would need confirmation. We cannot state with confidence whether the lobes also carry a magnetic field.

3.2 NGC 7027

The 450 μ m jiggle map of the young planetary nebula NGC 7027 (Fig. 2) and its near environment covers a field of about 40×36 arcsec². The central star is surrounded by an ionized area of ~ 283 arcsec², which is in turn enclosed by a thin atomic and molecular layer that is seen for instance in the H₂ emission observed by

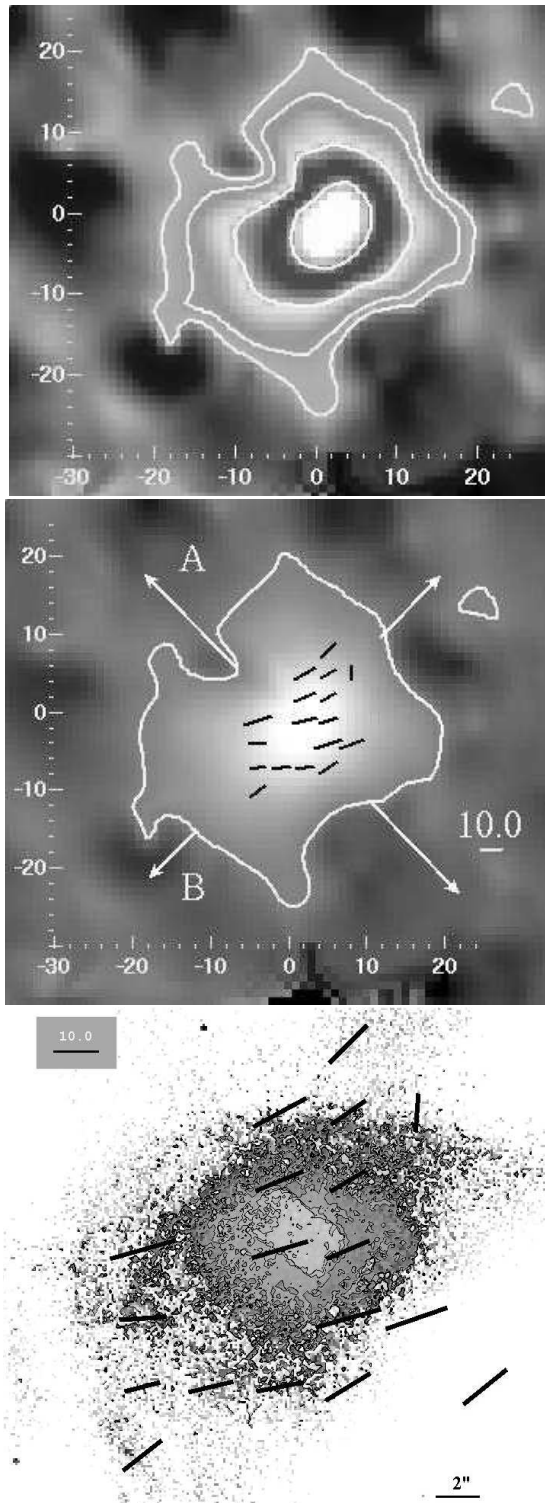


Figure 1. Scuba $850\mu\text{m}$ results on NGC 6537. North on the top and East on the left. The axes give the image scale in arcseconds. *Top panel:* the $850\mu\text{m}$ continuum map of NGC 6537, with contours at 1%, 2% ,5% and 10% of the peak. *Middle panel:* Magnetic field orientation. The general outflow direction of the nebula is indicated by A and the equatorial plane by B. The polarization vector scale on the left is set at 10%. *Bottom panel:* Extinction map presented by Matsuura et al. (2005). The highest levels of extinction occur at ~ 4 arcsec from the central star with $E(H\beta - H\alpha) > 2$ mag, coincident with the dust emission in the $850\mu\text{m}$ map. The polarization vector scale is set at 10%. The magnetic field which coincides with the area of internal extinction, is mostly aligned along the equatorial plane, indicating a toroidal field. The dust alignment is perpendicular to the vectors displayed.

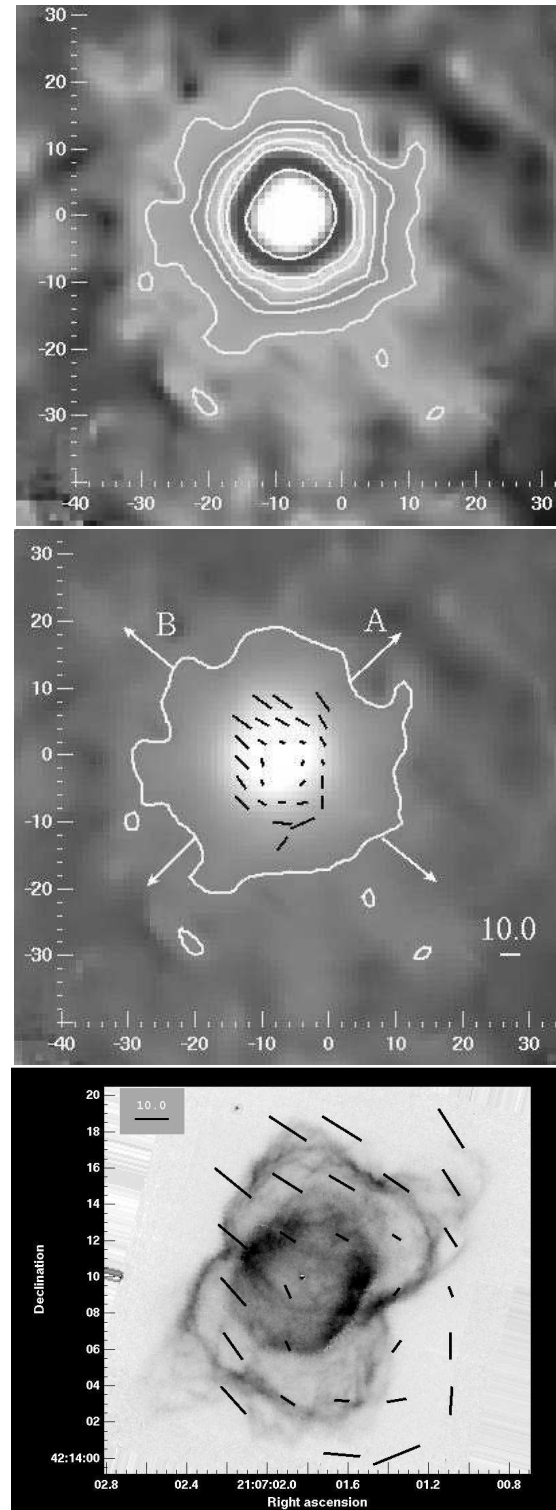


Figure 2. Scuba $450\mu\text{m}$ results on NGC 7027. North on the top and East on the left. The axes give the image scale in arcseconds. *Top panel:* The $450\mu\text{m}$ continuum map of NGC 7027. Contours are set from 1 to 5% and 10% of the peak. *Middle panel:* Magnetic field distribution. The general outflow direction is indicated by A and the equatorial plane by B. The polarization vector scale (showing the degree of polarization) is set at 10%. *Bottom panel:* The Scuba polarization vectors are shown on a continuum subtracted H_2 (color-inverted) map of NGC 7027 (North on the top and East on the left). The field is mostly directed along the equatorial plane. The central region shows much reduced polarization and the field orientation differs on the extreme western side.

Cox et al. (2002). A thin dark ring delineates the equatorial plane in optical images. The structure is better seen in the HST image (Fig. 2-bottom), which shows both the surrounding molecular layer (in H₂) and the inner ionized region. Latter et al. (2000) shows that the NW lobe is blue-shifted (closer) and the SW lobe is red-shifted.

The dominant direction of the magnetic field coincides with the equatorial plane. But this behaviour is mainly seen on the North-East side while the south-west part seems to be disturbed: the magnetic field may be “broken”. The degree of polarization is $8.9\% \pm 0.9\%$ towards the NE direction (or lobe) and $7.6\% \pm 1.3\%$ towards the SW. The degree of polarisation is much reduced in the center of the nebula and lacks a coherent direction here. This effect was also noted by Greaves (2002) and may indicate that coherence is lost in the ionized region.

3.3 CRL 2688

The proto-planetary nebula CRL 2688 (or Egg Nebula) is a bright carbon-rich bipolar object characterized by two pairs of searchlight beams superposed on a reflection nebula. The origin of the light beams has been suggested to be a very close stellar companion (Sahai et al. 1998; Kastner & Soker 2004), or the presence of dust layers reflecting the light of the central star (Goto et al. 2002). The bipolar reflection nebula shows a dark equatorial lane where a large amount of dust may be present.

The 850- μm is presented in Fig. 3-Top panels. It shows elongation in the direction of the polar outflows. The equatorial extent is less but at the lowest contour the torus is more extended on the eastern side. The extent is $\sim 60'' \times 40''$ although it is not clear precisely where the emission ends. The bright core at 850 μm shows a FWHM of $16 \times 14 \text{ arcsec}^2$, at a position angle of 25 degrees which is in the same direction as the outflow. We could not measure the core elongation at 450 μm due to the under-sampling. The spatial resolution is insufficient to separate the two light beams, but the width of the emission suggests that the dust traces the larger lobes which the light beams illuminate, and that these beams themselves are not present in the far-infrared data. (The elongation of the core is in fact along the line of one of the two beams only.)

CRL 2688 presents the highest number of polarization vectors in our sample. For this nebula, the under-sampled 450 μm map gives some additional and useful indications (even if we observe a lack of vectors due to this under-sampling). The polarization vectors cover the full nebular extent (seen at both wavelengths), as they do in NGC 7027. The degree of polarization is not uniform and strongly decreases near the center. This phenomenon is more visible in the 850 μm map, which suggests that beam depolarization may play a role. At 850 μm , the mean value of polarization of the region containing the bipolar lobes is about 3.2%, the outer region has a mean value of 8.8%, and the region of the dark lane shows a mean degree of polarization of 1.4%.

If we draw a line passing through the nebula in a longitudinal direction (NNE-SSW fig.3 bottom-left panel), we can see distinct behaviours of the magnetic field on either side of this line: on the eastern side, the orientation of \vec{B} is mainly in the direction of this line, while on the western side, the magnetic field appears perpendicular to it.

The 450- μm map (Fig. 3-bottom-right panel) shows the magnetic field at higher resolution, confirming the bimodal distribution. This map is under-sampled and only some positions in the nebula are covered. The map gives a suggestion of a superposition of a toroidal field and one aligned with the polar outflows. The field becomes less ordered towards the tip of the outflow direction, but

the emission here is faint and the uncertainties on the polarization vectors are larger.

The complicated magnetic morphology makes it likely that the dynamics have shaped significant parts of the field, rather than the magnetic field shaping the nebula. The structure may show the superposition of two components over most of the area of the source. The lack of polarization in the centre suggests that the bright core is not polarized, or its polarization is averaged out over the JCMT resolution. The outermost field vectors in the longitudinal direction are along the outflow, and this may indicate a field carried along by the outflow. This is most apparent in the north when looking at the outer vectors direction in the figure 3-bottom-left, in the south the outer vectors point towards the corresponding outflow so we assume that the magnetic field may be carried by this outflow.

The grain alignment, which is perpendicular to the direction of the magnetic field, is in the direction of the outflows on the western side. On the eastern side, the grain alignment is toroidal.

High resolution molecular images in the literature include IRAM CO J=2-1 data (Cox et al. 2000) and HST infrared H₂ images (Sahai et al. 1998). The continuum-subtracted H₂ image in Fig. 4, shows multiple jets, located both in the equatorial plane and towards the polar directions. The CO data show these jets to be the tip of flows originating much closer to the star. These jets all fall within the Scuba 850- μm core, indicating that indeed structure is present on scales much smaller than the JCMT beam size. Thus, beam dilution and beam-depolarization of the magnetic field is likely.

We note that the elongation visible in the Scuba image, on the eastern side, is in the same direction as the largest molecular subject E2 in Fig.4, or A1 in Cox et al. (2000) (but the Scuba structure is much larger). The polarization vectors seem unaffected. On the western side, both the molecular and the Scuba images indicate a smaller extent of the envelope. The polar outflows as seen in the molecular lines do not show the light beams, but instead show relatively well-collimated lobes. The lobes are brighter in the north. The polar lobes in the Scuba image are consistent with this, both in direction and in brightness, but again are much larger than seen in the molecules. The molecular emission shows the wind-blown cavities, while the Scuba emission arises in the surrounding shells.

3.4 NGC 6302

This oxygen-rich planetary nebula (Pottasch & Beintema 1999) is a proto-typical butterfly-type nebula. It shows two extended lobes that result from a bipolar outflow, with a dark lane in the center. It has been studied by Meaburn & Walsh (1980), Meaburn et al. (2005), Matsuura et al. (2005) and Casassus et al. (2000).

The Scuba observations were optimized for 450- μm . They show a bright core, of FWHM $14 \times 12 \text{ arcsec}^2$ (larger than the beam), with the long axis in the north-south direction, with an extension towards the south-southeast (Fig.5). We underline the fact that the long horizontal line in the eastern part of the nebula and the long vertical line in the South-West (Fig.5 bottom panel), are artifacts from the HST image and not Scuba polarization vectors. The arcs seen at 25 arcsec are likely part of the diffraction pattern from the very bright core. The polarimetric data obtained at 450 μm shows only five polarization vectors. They do not line up with either the dark lane or the outflow. However, they are fairly well aligned with the ellipsoidal radio source in the center of the nebula. The radio nebula shows the inner ionized region, confined by the dense torus: the elongation is perpendicular to the torus.

The difference in position angle of the inner torus with the

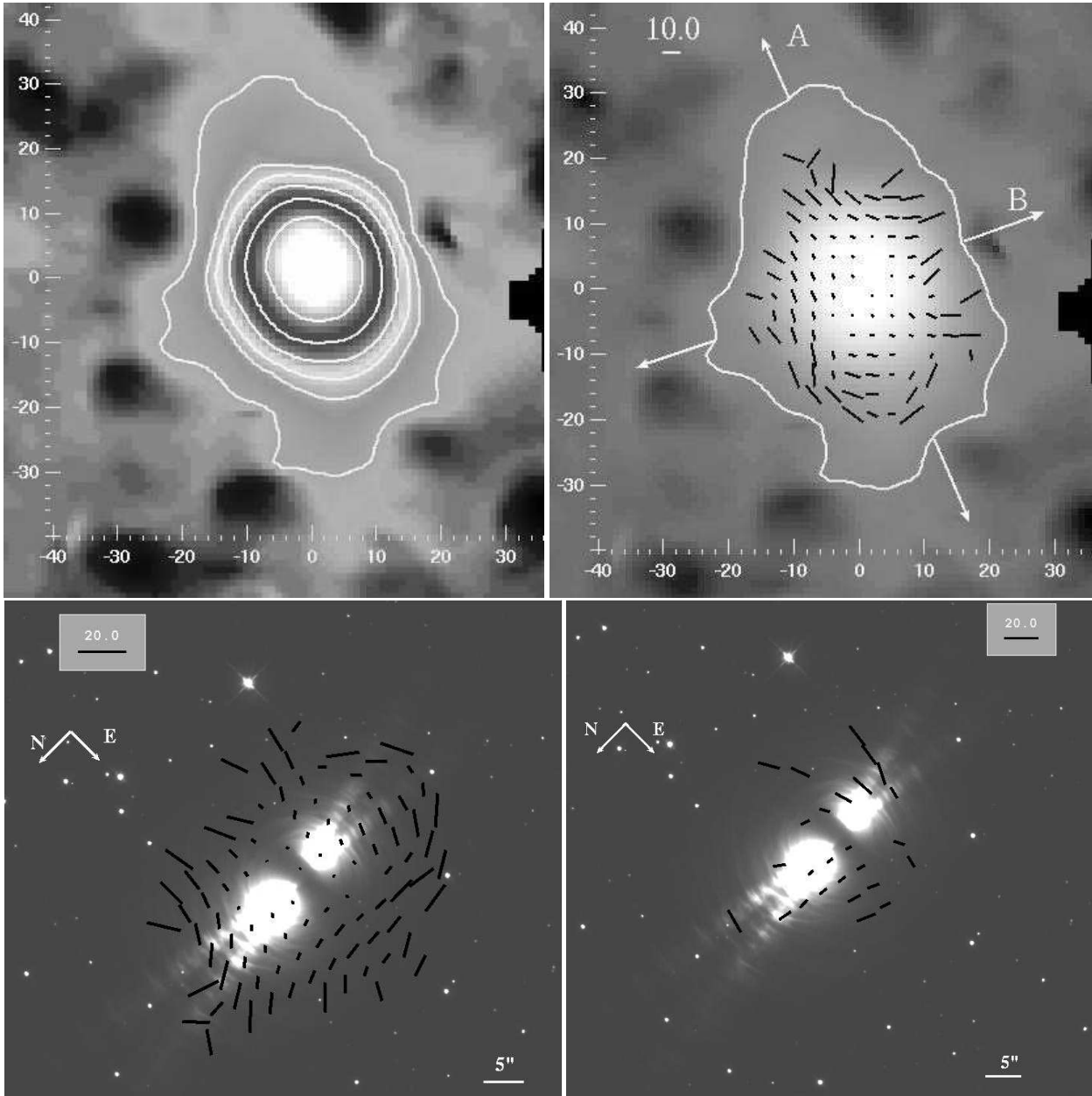


Figure 3. Scuba 850 and 450 μm results on CRL2688. North on the top and East on the left. The axes give the image scale in arcseconds. *Top left panel:* The 850 μm map of CRL 2688, with contours from 1 to 5% and 10% of the peak. *Top right panel:* The 850- μm vector polarization showing the magnetic field orientation. The general outflow direction is indicated by A and the equatorial plane by B. The polarization vector scale (showing the degree of polarization) is set at 10%. *Bottom panels:* HST images (WFPC2, filter F606W) with the overlaid magnetic field corresponding to the 850 μm map (left) and 450 μm map (right). The dust continuum is elongated along the outflows. The field shows a complicated structure with components along the outflow and along the equatorial plane. The polarization vector scale (showing the degree of polarization) is set at 20% for both maps.

dark lane is interpreted as a warped disk (Matsuura et al. 2005). Further from the center the outflows have different position angles, and eventually become east-west in the outer bipolar lobes. The 450- μm polarization indicates that the magnetic field may be oriented in the direction of the inner outflow.

We have no data for magnetic fields elsewhere in the outflows even at 850 μm .

4 DISCUSSION AND CONCLUSION

The sub-millimeter observations of the four post-AGB objects reveal new information regarding the distribution of the magnetic fields, the dust emission and the link between the two components.

Extended dust emission was seen for all four nebulae. For CRL 2688, the large polar lobes have been detected. The orientation of its polar lobes is along only one of the two light beams. The equatorial emission is also extended, and shows an asymmetry which is correlated with the appearance of the (much more compact) equatorial jets. These jets originate close to the star and it is

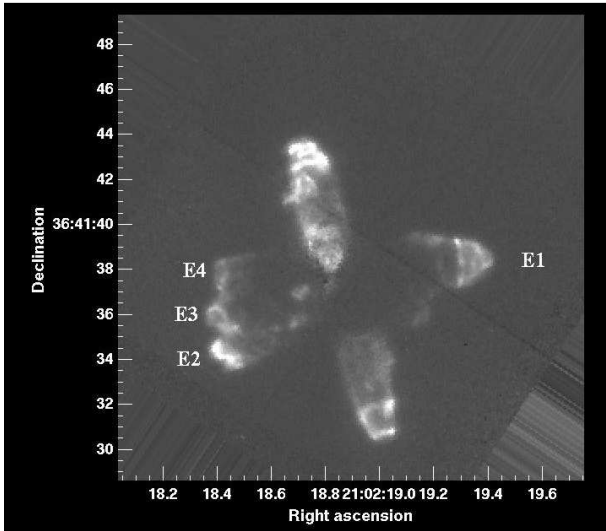


Figure 4. Continuum-subtracted H_2 (HST) image showing the jets in CRL 2688. [North at the top and East at the left]. They are named as in Sahai et al (1998). The jets are all located within the compact $850\text{-}\mu\text{m}$ source, and the some perturbations seen in the Scuba data can be related to the “sub-jets” E2 or A1.

Name	Band (μm)	Deg (%)	Angle (deg)
NGC 6537	850	11.2 ± 2.2	26.5 ± 5.7
NGC 6302	450	11.4 ± 1.6	32.7 ± 4.6
NGC 7027	450	8.2 ± 0.9	-18.5 ± 3.7
CRL2688	850	6.8 ± 1.0	-22.6 ± 4.5

Table 1. Mean values of the polarimetric parameters for the Post-AGB objects, Deg: degree of polarization, Angle: position angle of the polarization. These values concern the main band studied for each nebula.

unlikely that they are affected by structures at much larger scales. Instead, the jets may affect the dust emission through heating. In NGC 6537, an asymmetry in the dust correlates with differences in the extinction map, suggesting that here the Scuba map shows a true asymmetry in the dust distribution.

The presence of detectable polarization shows that at least some of the dust grains are not spherical.

4.1 Targets

Polarization is detected for all four nebulae. This in itself suggests that magnetic fields are common for these types of objects. It is thus important to discuss what types of objects were selected.

First, the four targets are all bipolar nebulae. The least pronounced morphology is shown by NGC 7027, but even here the molecular maps clearly show the underlying bipolar structure. We do not have information on the existence of magnetic fields in less bipolar (e.g. elliptical or spherical) nebulae.

Second, although three of the nebulae have very hot central stars and ionized cores, all have extended molecular envelopes. It is argued above that the detected fields are located in the molecular or atomic regions. The presence of molecular envelopes around ionizing stars indicates very dense nebulae, and therefore very high mass loss rates on the AGB.

Third, the dense nebulae with relatively small ionized regions imply that their stars have evolved to high temperatures before the

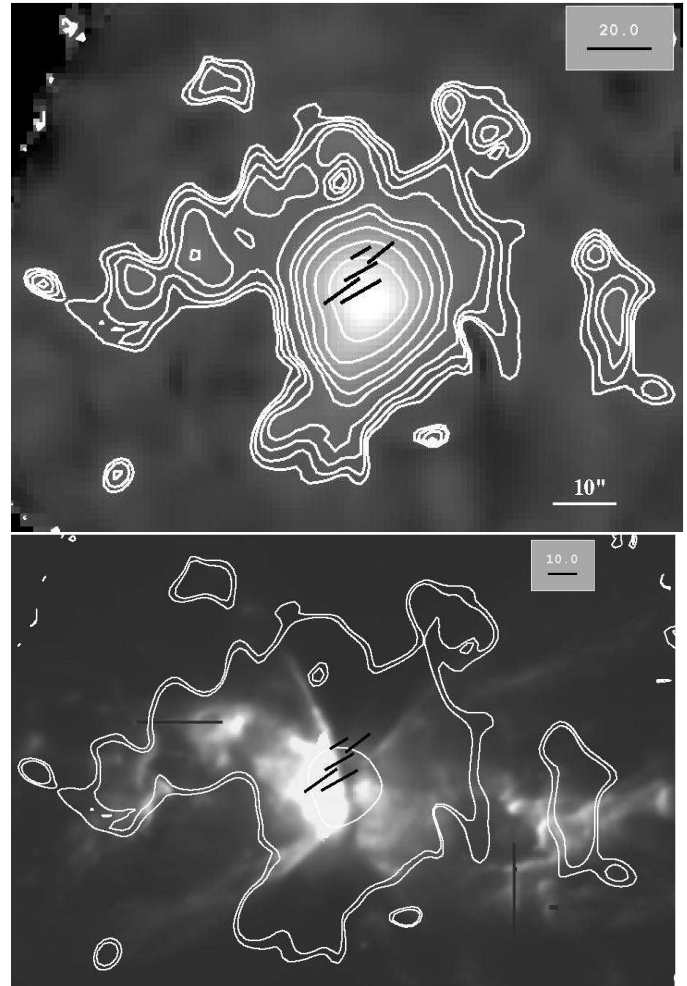


Figure 5. Scuba $450\mu\text{m}$ results on NGC 6302. North on the top and East on the left. *Top panel:* The map shows the magnetic field orientation on the planetary nebula with contours from 1 to 5%, 10%, 20% and 25% of the peak. The polarization vector scale (showing the degree of polarization) is set at 20%. Note that the arcs seen 20 arcsec out are part of the beam side lobes of the very bright core. *Bottom panel:* $450\mu\text{m}$ Scuba map of NGC 6302 overlaid on the F656N band HST image (WFPC2). North on the top and East on the left. The external hexagonal contours do not belong to the star but are representative of the bolometers. The main Eastern outflow seen on the submillimeter image coincides with the one observed with the HST. Note that the arcs seen 25 arcsec out are part of the beam side lobes and the two long lines (horizontal and vertical) on both sides of the nebula, are artifacts from the HST image and not polarization vectors.

nebulae have had time to expand significantly. Such fast evolution is characteristic for high-mass central stars. The cooler object (CRL 2688) may have a lower mass, but the fact that it has become a carbon star suggests it still has a relatively higher initial mass ($M_i \gtrsim 3M_\odot$), as lower-mass stars experience insufficient dredge-up to become carbon rich. For NGC 6302, a progenitor mass of $4\text{--}5M_\odot$ has been suggested, based on the mass of the circumstellar envelope (Matsuura et al. 2005). The precise initial masses are not well determined, but high mass progenitors appear likely for all four objects.

Thus, the result of the survey can be interpreted that magnetic fields tend to be present for high mass progenitors evolving into bipolar nebulae, and that the fields are detectable while the nebulae still have molecular envelopes.

4.2 Field location and orientation

Overall, we see fields aligned with the polar directions and/or toroidal fields in the equatorial plane. Assuming that the dust in the polar flows originates from the dust reservoir in the disk or torus, this suggests that the field also originates there. The alignment with the polar flow is interpreted that the gas carries the field with it.

NGC 6302 is the only source in our sample without evidence for a toroidal field. This nebula has a complicated morphology with a warped disk and the nebula is oriented at 45 degrees with respect to the equatorial dust lane. It is therefore difficult to ascertain the alignment of the field with any particular morphological component. However, alignment with the radio core seems most likely.

The other nebulae show evidence for toroidal field components. We therefore suggest that the initial configuration of the field is toroidal, and is located in the equatorial torus.

The polarization in all cases appears to be seen in the neutral/molecular regions. Towards the central, ionized regions, the percentage of linear polarization is much reduced. This may in part be because of the beam averaging over regions of different polarizations, but the ionized regions may also be expected to lose a directional field (non-constancy of \vec{B}). The reason for the absence of a detectable magnetic field in the ionized region can also be explained by the lack of dust (so \vec{B} is not carried). For NGC 6302, the field is aligned with the ionized core but is likely located around rather than within the core.

Polarization will not be detected if the field is oriented along the line of sight. This is expected for a toroidal fields near the tangential points of the torus. This may be present especially in CRL 2688, where two components are found at different locations.

4.3 Chemistry

The sample includes two oxygen-rich nebulae (NGC 6537 and NGC 6302, both PNe with hot central stars) and two carbon-rich nebulae (NGC 7027 and CRL 2688: the latter is the cooler post-AGB nebula in our sample). This sample is too small to draw general conclusions. However, we point out the following points of interest, for future study.

- The O-rich PNe both present collimated magnetic fields concentrated near the central star. In both cases, we have an organized magnetic field in the central region, resistant to distortion effects, but do not detect more distant fields.
- The two carbon-rich nebulae show extended fields covering their entire nebula. In both nebulae, the magnetic field is more disorganized than in the two O-rich stars.

The question whether there is a chemistry-related origin to these behaviours is valid, but cannot be answered with the current sample. Dust chemistry could play a role. First, carbon grains tend to be smaller than silicate grains. Larger grains may be more spherical, which would give less (or no) polarization. Both oxygen-rich nebulae show evidence for crystalline ice (Molster et al. 2002) (strongest in NGC 6302), indicating coatings on the grains. Second, amorphous carbon grains may be intrinsically non-spherical, build up from graphitic carbon sheets.

For the O-rich nebulae, it is possible that only the hotter dust, above the ice evaporation temperature, leads to non-spherical grains and a polarized signal. Thus, a difference in polarization does not necessarily imply a difference in magnetic field structure.

Both O-rich nebulae show evidence for weak PAH emission in their central regions. The origins of the PAHs is not clear, but they

are seen only in irradiated regions. The continuum radiation from the dust component containing the PAHs is only seen at short wavelengths (warm dust) and contributes very little to the sub-mm flux (Kemper et al. 2002; Matsuura et al. 2005). Thus, the polarization signal is seen in the oxygen-rich grains, not the PAHs.

Iron needles could be considered as carriers of the polarization: in O-rich stars, some or most of the iron is incorporated in the silicate grains (olivines and pyroxenes: Ferrarotti & Gail 2001), but for a C/O ratio close to and above unity, solid iron and FeSi become more important (e.g., Ferrarotti & Gail 2002). Metallic, non-spherical iron grains may contribute to the NIR opacity in high mass-loss OH/IR stars (Kemper et al. 2002).

4.4 Comparison less evolved/ more evolved nebulae

The extent of the nebulae shows that the objects differ in age. The nebulae of CRL 2688 (Post-AGB) and NGC 7027 (young PN) are younger than NGC 6537 (PN) and NGC 6302 (PN). (The lobes of the last object extend to over 2 parsec across.)

Our submillimeter polarimetric data show that the magnetic field is better organized for the older nebulae. Assuming an originally toroidal field, later carried by the bipolar flows, the best organized field is expected if one component dominates. The bipolar flows are most massive early in the post-AGB evolution (Bujarrabal et al. 2001). As they diminish, the remaining field may become less confused. However, evolving dust characteristics may also play a role: dust grains become larger in older disks, and may show less polarization as a result. It is not possible with the current sample to separate evolutionary and chemical effects, but both are expected to occur.

4.5 Field strength and origin

The detected polarization contains information on the direction of the field, but not its strength. A method to obtain the field strength out of fluctuations in polarization was suggested by Chandrasekhar & Fermi (1953). Applying this method to our data leads to field strengths of the order of mG. This equation assumes that the magnetic field dispersion is caused by Alfvén waves. The applicability to our sources may be in doubt, as the dispersion may be dominated streaming motions.

In neutral-dominated media, Alfvén waves contribute if the collision times between ions and neutrals are shorter than the period of the Alfvén wave. This is the case for waves longer than

$$\lambda_A > \left(\frac{0.3}{\text{pc}}\right) \left(\frac{B}{0.1 \text{ mG}}\right) \left(\frac{10^4}{n}\right)^{3/2} \left(\frac{10^{-7}}{f_i}\right) \quad (1)$$

where n is the particle density per cm^3 , and f_i is the fractional ionization (Hildebrand 1996). For our sources, f_i may be high except in the densest regions of the tori. Assuming a typical source size of 0.05 pc, and a field strength of a mG, Alfvén waves may contribute if $f_i > 10^{-4}$. This is a plausible value for the outflows.

Previous observations of OH Zeeman splitting has shown field strengths in OH/IR stars and post-AGB stars of a few mG at $3 \times 10^{15} - 2 \times 10^{16} \text{ cm}$ from the stars (Bains et al. 2004, 2003). Much larger values have been inferred from water masers: several Gauss at $\sim 2 \times 10^{14} \text{ cm}$ (Vlemmings et al. 2005). The difference is consistent with a dipole field, which gives an r^{-3} dependence, and less consistent with a solar-type field r^{-2} . Water masers trace high density clumps and the measured field strengths may not be fully representative of the surrounding areas.

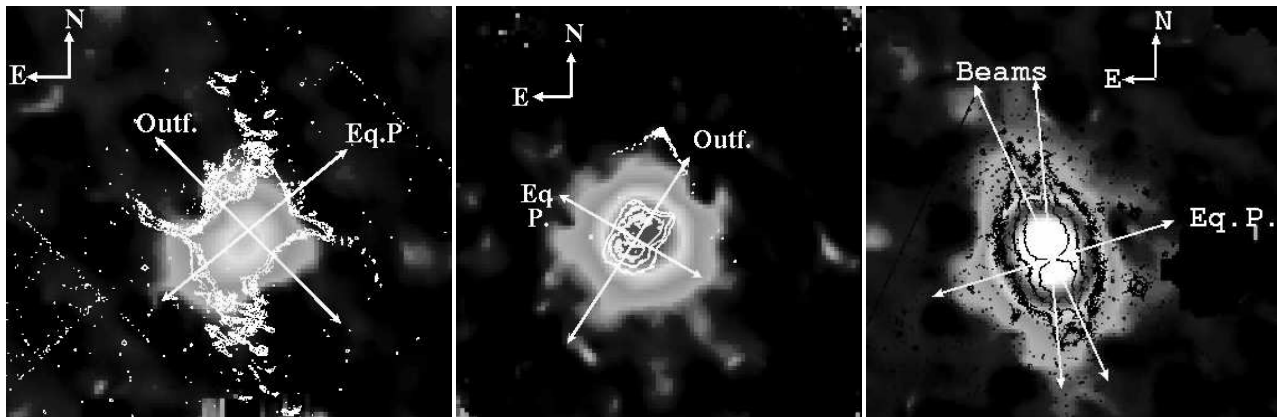


Figure 6. Location of the Scuba dust emission, compared to the HST images (contours). We present respectively NGC 6537, NGC 7027 and CRL 2688. NGC 6302 is shown in Fig.5 (bottom panel).

Assuming we look at typical distances of 5 arcsec at 1 kpc, our measurements are at $\sim 5 \times 10^{16}$ cm from the stars. Compared to the OH and water masers, one would expect a field of 1mG or less at this distance. This suggest that the direction changes in the field are due to streaming motions, rather than Alfvén waves.

The grains become aligned with the magnetic field with the Davis-Greenstein mechanism. The time scale for this to occur is (Kruegel 2003, Ch. 11)

$$t_{\text{rel}} \propto B^{-2}$$

and, for fields of the order of a few mG, is typically 10^6 yr. The age of the nebulae is $\sim 10^4$ yr. For this time scale, the alignment of the dust with the magnetic field requires fields in excess of those seen from OH maser emission. The alignment is therefore likely to originate close to the central star, at $r < 10^{15}$ cm, and is maintained while the nebula expands.

4.6 Evolution

For OH/IR stars, evidence for dipole fields has been presented by, e.g., Vlemmings et al. (2005). For more evolved stars, in the early post-AGB evolution, the presence of both toroidal (IRAS 20406+2953) and poloidal (OH17.7-2.0) fields are inferred from OH observations (Bains et al. 2004, 2003). The poloidal fields arise from a stretched dipole. For the even later evolutionary stage studied here, a strong toroidal field component is found, combined with a poloidal field.

A toroidal field can form out of a dipole field by rotation. This already makes it likely that the formation of the torus and the formation of the toroidal field are related. A binary companion can be the source of the required angular momentum. Rotation of the star itself is less likely, as its angular momentum can be expected to be lost early on in the mass loss. A binary companion, on the other hand, can deposit its angular momentum during the time of the peak superwind, at the end of the AGB mass loss.

The fields detected via OH and H₂O masers have been claimed to be strong enough to dominate the dynamics of the nebula (Bains et al. 2004; Vlemmings et al. 2005). Soker (2006) argues that fields of this magnitude cannot be generated by the star itself, and should be attributed to a companion. Based on this, the basic shaping mechanism of the nebula is found in binarity. However, once the strong fields have been generated, they would be a signif-

icant factor in the further evolution of the nebula towards the PN phase.

4.7 Summary

We present the discovery of magnetic fields in four bipolar post-AGB stars (NGC 6537, NGC 7027, NGC 6302 and CRL 2688). This confirms the earlier work of Greaves (2002) for two of these. The fields are mapped at high resolution (for sub-mm), using either 450 or 850 μm . The sub-mm emission traces the extended emission. In CRL 2688, we find evidence for the polar lobes which contain the well-known search beams.

All objects show polarization indicative of grain alignment by magnetic fields. Toroidal fields are found for three objects, and poloidal fields for two (CRL 2688 shows evidence for both). The alignment of the field with nebula is least certain for NGC 6302, where the nebula shows a multipolar structure. Our results suggests that magnetic fields are common in these types of targets: bipolar nebulae with intermediate-mass progenitors. The fields are long lived as they are observed over different evolutionary stages.

The data also show evidence for elongated grains. The polarization is stronger and more extended for the carbon-rich nebulae. This may show that amorphous carbon grains are intrinsically non-spherical, e.g. the sheet-like structure of graphite. The oxygen-rich nebulae show polarization only in their central regions. This is interpreted in that the dust grains in the torii are larger and more spherical.

The poloidal fields in the polar flows suggest that here the field is carried along by the flow and that these flows are not magnetically confined. The toroidal components in the torus may be more important, for the dynamics. As the fields in AGB stars are dipole-like, the toroidal field structure appears to be a later phase of evolution. We suggest that this transition occurs when the equatorial field is wound up through the interaction with a companion. Following Soker (2006), we suggest that the original shaping agent is a binary companion. Once the field has been wound up, it may however become dynamically important for the subsequent nebular evolution.

ACKNOWLEDGEMENTS

L.S. thanks Mikako Matsuura for many useful comments and for providing the reduced HST data. The James Clerk Maxwell Telescope is operated by The Joint Astronomy Centre on behalf of the Particle Physics and Astronomy Research Council of the United Kingdom, the Netherlands Organisation for Scientific Research, and the National Research Council of Canada.

REFERENCES

- Bains I., Gledhill T. M., Richards A. M. S., Yates J. A., 2004, in ASP Conf. Ser. 313: Asymmetrical Planetary Nebulae III: Winds, Structure and the Thunderbird The Magnetic Field and Maser Structure in the Proto-Planetary Nebula IRAS 20406+2953. pp 186–+
- Bains I., Gledhill T. M., Yates J. A., Richards A. M. S., 2003, MNRAS, 338, 287
- Balick B., Frank A., 2002, ARAA, 40, 439
- Barnbaum C., Morris M., Kahane C., 1995, ApJ, 450, 862
- Blackman E. G., Frank A., Markiel J. A., Thomas J. H., Van Horn H. M., 2001, Nature, 409, 485
- Bond H., Murdin P., 2000, Encyclopedia of Astronomy and Astrophysics
- Bujarrabal V., Castro-Carrizo A., Alcolea J., Sánchez Contreras C., 2001, A&A, 377, 868
- Casassus S., Roche P. F., Barlow M. J., 2000, MNRAS, 314, 657
- Chandrasekhar S., Fermi E., 1953, ApJ, 118, 113
- Ciardullo R., Sigurdsson S., Feldmeier J. J., Jacoby G. H., 2005, ApJ, 629, 499
- Corradi R. L. M., Schwarz H. E., 1993, A&A, 269, 462
- Cox P., Huggins P. J., Maillard J.-P., Habart E., Morisset C., Bachiller R., Forveille T., 2002, A&A, 384, 603
- Cox P., Lucas R., Huggins P. J., Forveille T., Bachiller R., Guilleoteau S., Maillard J. P., Omont A., 2000, A&A, 353, L25
- Cuesta L., Phillips J. P., Mampaso A., 1995, A&A, 304, 475
- De Marco O., Bond H. E., Harmer D., Fleming A. J., 2004, ApJ, 602, L93
- De Marco O., Moe M., 2006, ApJ, in press
- Ferrarotti A. S., Gail H.-P., 2001, A&A, 371, 133
- Ferrarotti A. S., Gail H.-P., 2002, A&A, 382, 256
- Goto M., Kobayashi N., Terada H., Tokunaga A. T., 2002, ApJ, 572, 276
- Greaves J. S., 2002, A&A, 392, L1
- Greaves J. S., Holland W. S., Jenness T., Chrysostomou A., Berry D. S., Murray A. G., Tamura M., Robson E. I., Ade P. A. R., Nartallo R., Stevens J. A., Momose M., Morino J.-I., Moriarty-Schieven G., Gannaway F., Haynes C. V., 2003, MNRAS, 340, 353
- Greaves J. S., Holland W. S., Minchin N. R., Murray A. G., Stevens J. A., 1999, A&A, 344, 668
- Hildebrand R. H., 1996, in Roberge W. G., Whittet D. C. B., eds, ASP Conf. Ser. 97: Polarimetry of the Interstellar Medium Problems in Far-Infrared Polarimetry. pp 254–+
- Hildebrand R. H., Davidson J. A., Dotson J. L., Dowell C. D., Novak G., Vaillancourt J. E., 2000, PASP, 112, 1215
- Holland W. S., Robson E. I., Gear W. K., Cunningham C. R., Lightfoot J. F., Jenness T., Ivison R. J., Stevens J. A., Ade P. A. R., Griffin M. J., Duncan W. D., Murphy J. A., Naylor D. A., 1999, MNRAS, 303, 659
- Huggins P. J., Manley S. P., 2005, A&A, 117, 665
- Kastner J. H., Soker N., 2004, in ASP Conf. Ser. 313: Asymmetrical Planetary Nebulae III: Winds, Structure and the Thunderbird The Egg Nebula (AFGL 2688): Deepening Enigma. pp 57–+
- Kemper F., de Koter A., Waters L. B. F. M., Bouwman J., Tielens A. G. G. M., 2002, A&A, 384, 585
- Kemper F., Molster F. J., Jäger C., Waters L. B. F. M., 2002, A&A, 394, 679
- Kruegel E., 2003, The physics of interstellar dust. IoP Series in astronomy and astrophysics (IoP: Bristol, UK)
- Latter W. B., Dayal A., Bieging J. H., Meakin C., Hora J. L., Kelly D. M., Tielens A. G. G. M., 2000, ApJ, 539, 783
- Matsuura M., Zijlstra A. A., Gray M. D., Molster F. J., Waters L. B. F. M., 2005, MNRAS, 363, 628
- Matsuura M., Zijlstra A. A., Molster F. J., Waters L. B. F. M., Nomura H., Sahai R., Hoare M. G., 2005, MNRAS, 359, 383
- Matt S., Balick B., Winglee R., Goodson A., 2000, A&A, 32, 743
- Meaburn J., López J. A., Steffen W., Graham M. F., Holloway A. J., 2005, ApJ, 130, 2303
- Meaburn J., Walsh J. R., 1980, MNRAS, 193, 631
- Molster F. J., Waters L. B. F. M., Tielens A. G. G. M., Barlow M. J., 2002, A&A, 382, 184
- Pottasch S. R., Beintema D. A., 1999, A&A, 347, 975
- Riera A., García-Lario P., Manchado A., Suárez O., García-Hernández A., Guerrero M. A., 2003, in Revista Mexicana de Astronomia y Astrofisica Conference Series GLMP 621: a Binary Planetary Nebula. pp 97–99
- Sahai R., Hines D. C., Kastner J. H., Weintraub D. A., Trauger J. T., Rieke M. J., Thompson R. I., Schneider G., 1998, ApJ, 492, L163+
- Soker N., 2005, in Szczerba R., Stasinska G., Gorny S. K., eds, AIP Conf. Proc. 804: Planetary Nebulae as Astronomical Tools Can We Ignore Magnetic Fields in Studies of PN Formation, Shaping and Interaction with the ISM?. pp 89–94
- Soker N., 2006, A&A, 118, 260
- Vlemmings W. H. T., Diamond P. J., Imai H., 2006, Nature, 440, 58
- Vlemmings W. H. T., van Langevelde H. J., Diamond P. J., 2005, A&A, 434, 1029
- Zijlstra A. A., 2006, in Szczerba R., Mikalojewska J., eds, Symbiotic stars Binary central stars of planetary nebulae